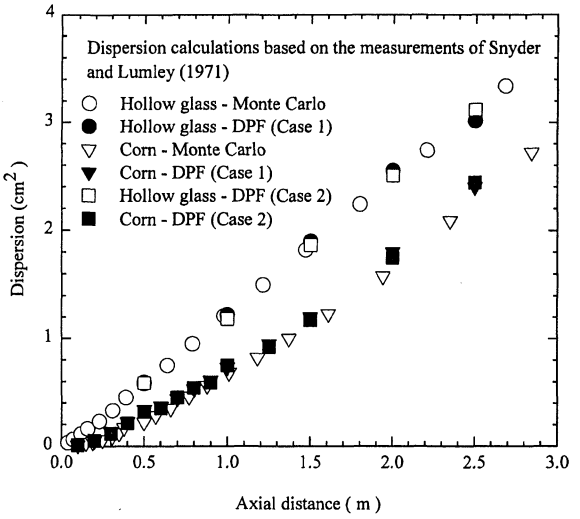

Fig. 1 Comparison of dispersion calculations using Monte Carlo and DPF methods.

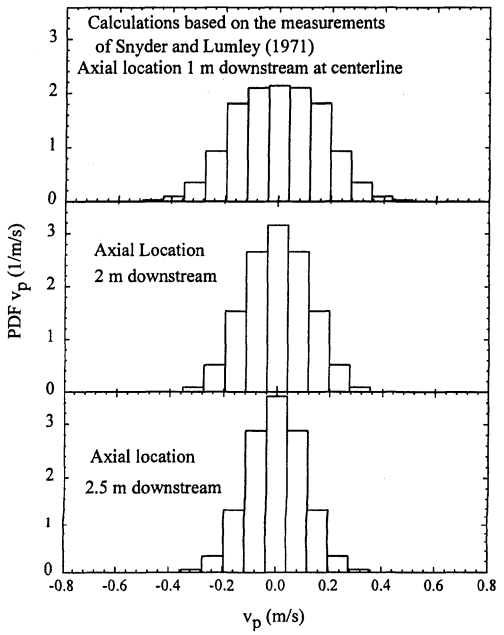

Fig. 2 PDFs of particle radial velocity using the DPF method.

The results of the DPF dispersion calculations are shown in Fig. 1 and have the same accuracy as the Monte Carlo simulations. The higher number of realizations used in the DPF method makes it substantially more computationally expensive than the grid-independent Monte Carlo simulations used for the present dispersion calculations. Dispersion results are also shown for $I \times J \times P \times Q = 11^4$ parcels (case 2: $I = J = P = Q = 11$) in Fig. 1. The level of discretization of the PDFs using 11 bins is adequate for the present calculation. The accuracy of calculations for a level of discretization will depend on the rms fluctuations (width of the PDFs). The PDFs of particle cross-stream velocities for hollow glass at downstream locations using the DPF method are shown in Fig. 2 and are well resolved.

Conclusions

A DPF method is applied to particle dispersion calculations in a turbulent two-phase flow and provides accurate simulations with low statistical noise. The larger number of computational parcels makes it more expensive than the present Monte Carlo simulation. However, the DPF method is capable of providing full field information and higher-order moments and correlations for dependent variables without any increase in computational expense and avoids the use of random number generators and constant mapping of a variable to its CDF for sampling. Also, important events that occur with low probability can be adequately simulated. The possibility of reducing computational expense by using recursive methods for nonlinear problems needs to be investigated. The DPF method (with improvements in computational efficiency) could be applied in applications where the dispersion/evaporation/mixing processes are critical and are uncoupled from the combustion process.

References

[1]Faeth, G. M., "Evaporation and Combustion of Sprays," *Progress in Energy and Combustion Science*, Vol. 9, Pergamon, New York, 1983, pp. 1–76.

[2]Litchford, R. J., and Jeng, S. M., "Efficient Statistical Transport Model for Turbulent Particle Dispersion in Sprays," *AIAA Journal*, Vol. 29, No. 9, 1991, pp. 1443–1451.

[3]Gosman, A. D., and Ioannides, E., "Aspects of Computer Simulation of Liquid-Fueled Combustors," AIAA Paper 81-0323, Jan. 1981.

[4]Berlemont, A., Desjonqueres, P., and Gouesbet, G., "Particle Lagrangian Simulation in Turbulent Flows," *International Journal of Multiphase Flow*, Vol. 16, No. 1, 1990, pp. 19–34.

[5]Solomon, A. S. P., Shuen, J. S., Zhang, Q. F., and Faeth, G. M., "Structure of Nonevaporating Sprays, Part I: Drop and Turbulence Properties," *AIAA Journal*, Vol. 23, No. 11, 1985, pp. 1724–1730.

[6]Sivathanu, Y. R., and Gore, J. P., "A Discrete Probability Function Method for the Equation of Radiative Transfer," *Journal of Quantitative Spectroscopy and Radiative Transfer*, Vol. 49, No. 3, 1993, pp. 269–280.

[7]Snyder, W. H., and Lumley, J. L., "Some Measurements of Particle Velocity Autocorrelation Functions in a Turbulent Flow," *Journal of Fluid Mechanics*, Vol. 48, 1971, pp. 41–71.

[8]Dutta, P., "A Study of Turbulent Lean Premixed Prevaporized Combustion with Emphasis on Fuel Dispersion," Ph.D. Thesis, School of Mechanical Engineering, Purdue Univ., West Lafayette, IN, Dec. 1995.

Buckling and Postbuckling Behavior of Stiffened Composite Panels Loaded in Compression

I. C. Lee,* C. G. Kim,† and C. S. Hong‡
Korea Advanced Institute of Science and Technology, Taejon 305-701, Korea

Introduction

STIFFENED composite panels are extensively used in aircraft and other structural components to satisfy requirements of increased stiffness, reduced weight, and stability. Since the buckling of stiffened panels does not mean the total failure or collapse of structure, it has been found to be efficient to permit buckling of stiffened panels under the collapse load, i.e., postbuckling ultimate load. Therefore, it is essential to investigate the postbuckling behavior and failure characteristics of stiffened composite panels. However, it is not straightforward to evaluate postbuckling behavior of composite structures because of the complexities in predicting their performance when failure and structural degradation take place. Most of the previous buckling studies in analysis have focused on the buckling or initial postbuckling behavior.[1–3] The effect of failure on the postbuckling behavior was considered in a limited number of papers.[4] In most of the previous experimental studies,[3,4] the stiffened panels have been cocured without ply overlap in the junction part

Received May 16, 1996; revision received Sept. 10, 1996; accepted for publication Sept. 14, 1996; also published in *AIAA Journal on Disc*, Volume 2, Number 1.

*Research Assistant, Department of Aerospace Engineering.

†Associate Professor, Department of Aerospace Engineering. Senior Member AIAA.

‡Professor, Department of Aerospace Engineering. Senior Member AIAA.

of the skin and the stiffeners. This type of stiffened panels have low postbuckling load carrying capacity due to the separation between the stiffener and the skin. Therefore, it is necessary to eliminate the separation by cocuring the stiffener and the skin in a continuous laminate.

In the authors' previous paper, an improved load-increment method based on the arc-length scheme was presented, and the postbuckling behavior of composite laminated cylindrical panels under compression was investigated.[5,6] A progressive failure analysis based on the maximum stress criterion and the complete unloading model was also introduced into the nonlinear finite element analysis.[7] In this Note, this finite element program was applied to stiffened composite panels under axial compression, and the buckling and postbuckling behavior of composite panels was characterized. The cocured stiffened panel, of which the stiffeners were manufactured in continuous laminate with the skin, was tested. The finite element results were compared with experimental results for I-stiffened panels.

Finite Element Analysis

The eight-node degenerated shell element is used for the modeling of stiffened panels, and the first-order shear deformation theory is adopted in the nonlinear finite element analysis.

To estimate the failure load of stiffened composite panels for each failure mode, the maximum stress criterion is applied to the average stresses in the principal material directions of each layer of each element. Also, to estimate the postbuckling load-carrying capacity conservatively, it is assumed that the stress corresponding to the failure mode of each layer is completely unloaded and the corresponding stiffness is set to zero. This complete unloading failure model can be expressed by the following equations.

If fiber failure occurs, then

$$\sigma_1 = 0, \qquad E_1 = 0, \qquad \nu_{12} = 0, \qquad \nu_{13} = 0$$

If matrix failure occurs, then

$$\sigma_2 = 0, \qquad E_2 = 0, \qquad \nu_{21} = 0, \qquad \nu_{23} = 0$$

If shear failure occurs, then

$$\tau_{12} = 0, \qquad G_{12} = 0$$

The failure of each element in the model is estimated for the converged stresses during each load step, and the stress component corresponding to the failure mode is unloaded instantaneously. Therefore, if failure occurred at the previous load step, the force equilibrium is not satisfied at the first iteration of present load step, and an unbalanced force is induced due to the unloaded stress component. For the postbuckling failure analysis, the effect of the deformation due to the failure-induced unbalanced force should be introduced into the modified arc-length method.[7]

In case of modeling the skin and the stiffener with the degenerated shell elements, the incompatibility in degrees of freedom arises from the difference in local coordinates between the two elements to hold the adjacent nodes of the skin and the stiffener in common. The compatibility is enforced to the common nodes by equalizing the displacement in the global x, y, and z directions and matching the rotation about the local unit vector as shown in Fig. 1.

Experiment

The panel was fabricated from graphite/epoxy prepreg, and the material properties used in this study were $E_1 = 130.0$ GPa, $E_2 = E_3 = 10.0$ GPa, $G_{12} = G_{13} = 4.85$ GPa, $G_{23} = 3.62$ GPa, $\nu_{12} = \nu_{13} = 0.31$, $\nu_{23} = 0.52$, $X_T = 1933$ MPa, $X_C = 1051$ MPa, $Y_T = 51$ MPa, $Y_C = 141$ MPa, and $S = 61$ MPa.

The geometry, dimension, and boundary conditions of the panels are shown in Fig. 2a. As shown in Fig. 2b, the stiffened panel configuration consists of the two I-shaped stiffeners having the lay-up sequence of $[0/90/45/0/-45]_S$ for web and cap. The web and cap of the stiffener were formed by the continuous lay-up of skin, $[0/90/\pm 45]_S$. Two 0-deg plies for the flange were inserted into the skin, and one of them was continued to the web and cap. As a result,

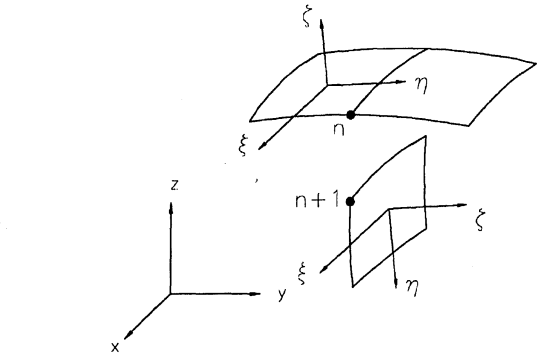

Fig. 1 Constraints for skin and stiffener node connection: $u^n = u^{n+1}$, $v^n = v^{n+1}$, $w^n = w^{n+1}$, and $\beta_\xi^n = \beta_\xi^{n+1}$.

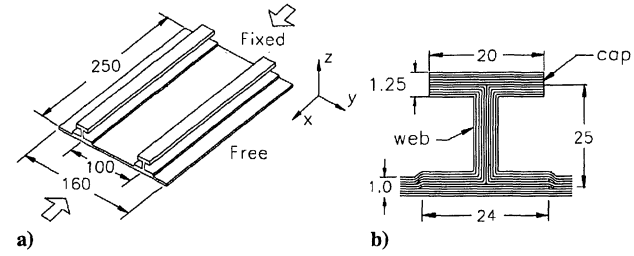

Fig. 2 Panel geometry, dimensions, and boundary conditions. Units are in millimeters.

the flange part including the skin has the same lay-up sequence of the web and cap. The stiffeners of the panels were cocured with the skin. That is to say, the stiffeners were manufactured in a body with the skin to eliminate the separation between stiffener and skin, whereas the stiffeners were formed without the ply overlap to the skin in the conventional fabrication of stiffened panels. Unidirectional tape fillers were inserted into the intersection between web and skin or cap. After cocuring, the panels were inspected using C-scan and no significant defects were detected. The loaded ends of the panels were potted in the casting resin, and they were machined flat and parallel to load the stiffened panel uniformly.

The panel was tested to failure in compression to investigate its postbuckling behavior. Linear strain conversion displacement transducers and strain gauges were used to measure the end shortening and the strain in the axial direction of the panel, respectively. Out-of-plane deflections were also monitored by the shadow moiré technique.

Results and Discussion

The load-end shortening curves obtained from experiment and finite element analysis are shown in Fig. 3. The end shortening u was normalized by the panel length L, and the applied load P was normalized by the prebuckling extensional stiffness EA of the panel. The experimental and analytical buckling loads are marked by the open circle and the open rectangle, respectively. The buckling load from experiment was determined by the stress-strain curves from back-to-back axial strain gauges attached at the center of the panel. The stiffened panel carried the applied load steadily to six or seven times of the buckling load in the postbuckling region. The separation between stiffener and skin was not found in the junction part even after the postbuckling ultimate load. Therefore, the high ratio of postbuckling ultimate load to buckling load P_{ul}/P_{cr} was obtained. This shows that the stiffened panel cocured in a body had an excellent postbuckling load-carrying capacity in spite of the relatively thin stiffener. The experimental buckling load as well as the postbuckling ultimate load are in good agreement with the analytical results as shown in Table 1. The exaggerated deformed pattern of the panel is shown in Fig. 4 for the solid marks of state A to D in Fig. 3. The deformation of the skin became large after buckling as the applied load increased, and maximum out-of-plane deflection was developed about four times of the skin

Table 1 Analytical and experimental results

Panel	Stiffener spacing, mm	Length/ stiffener spacing	EA, MN	P_{cr}/EA, $\times 10^3$	P_{ul}/EA, $\times 10^3$	P_{ul}/P_{cr}
Experiment analysis	100	2.5	18.10	0.483	3.392	7.02
S1	70	2.5	14.58	1.169	4.449	3.81
S2	100	2.5	17.01	0.589	3.959	6.72
S3	130	2.5	19.44	0.349	3.377	9.67

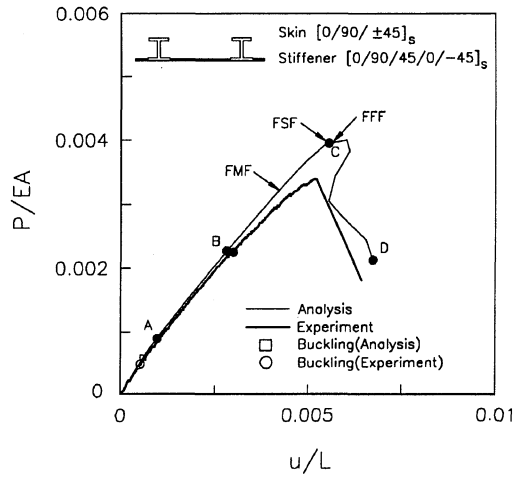

Fig. 3 Comparison of analytical and experimental results for load-end shortening curve.

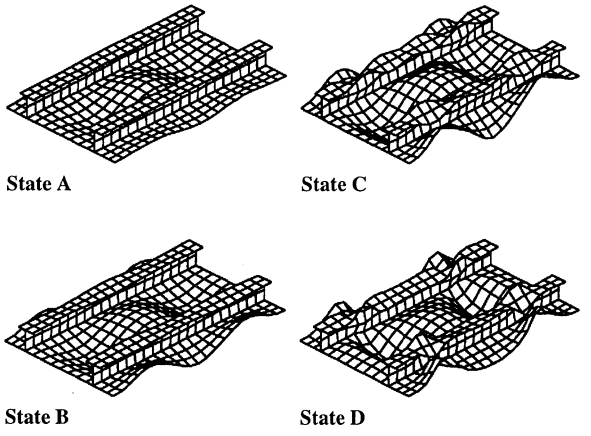

Fig. 4 Deformed shapes of stiffened panels.

thickness. However, the deformation of the stiffener was still small compared with that of the skin at state B. The applied load was carried mainly by the stiffener as the load increased in postbuckling region. The deformation of the stiffener became large after state B, and failures occur by the large deformation of the stiffener as the load increases in higher postbuckling range. Figure 5 shows the contour plot of the out-of-plane skin deflections generated from the finite element analysis and the photograph of the moiré fringe pattern corresponding to the out-of-plane deflections observed at the state B. These results show very good agreement in the postbuckling deformed shapes from both experiment and analysis.

In the failure analysis, the considered failure modes are matrix failure, shear failure, and fiber failure. The occurrence positions of the first ply failure of each mode are indicated on the load-end shortening curve in Fig. 3. The failure modes occurred at the load levels much higher than the buckling load. The tension matrix failure appeared first at the outer layer of the web due to the large out-of-plane deflections. This matrix failure hardly decreased the load-

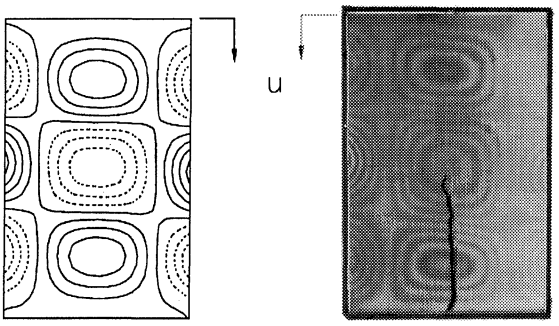

Fig. 5 Comparison of analytical and experimental results for the contour plots of out-of-plane deflection (dotted lines represent negative w): state B.

carrying capacity of the panel. As the applied load increased, the shear failure occurred mainly at the 45- or −45-deg layer, and then the fiber failure was generated by the compressive stress due to the in-plane force and bending moment at the outer layer of the panel. These failure modes induced the reduction in the stiffness of the panel abruptly. At last the load-carrying capacity of the stiffened panel was lost rapidly.

The effect of various stiffener spacings on buckling and postbuckling behavior is shown in Table 1. As would be expected, the model predicts lower buckling and ultimate failure loads for geometries with larger stiffener spacing. The ratio of postbuckling ultimate stress to buckling stress P_{ul}/P_{cr} decreased as the stiffener spacing decreased.

Conclusion

A modified arc-length method combined with the progressive failure model was used in the nonlinear finite element method. The finite element program was applied to stiffened composite panels under axial compression, and buckling and postbuckling behavior of the panels was characterized. The web and the lower part of cap of stiffener were fabricated by the continuous plies of the skin for cocuring the stiffened panel. Therefore, the separation between stiffener and skin was not found in the junction part even after postbuckling ultimate load, and the stiffened panel had excellent postbuckling load-carrying capacity. The analytical results on the buckling load, postbuckling ultimate load, and postbuckling deformed shape show good agreement with the experimental results for an I-stiffened panel.

References

[1]Dickson, J. N., Cole, R. T., and Wang, J. T. S.,"Design of Stiffened Composite Panels in the Post-Buckling Range," *Fibrous Composites in Structural Design*, edited by E. M. Lenoe, D. W. Oplinger, and J. J. Burke, Plenum, New York, 1980, pp. 313–327.

[2]Sheinman, I., Frostig, Y., and Segal, A., "PBCOMP Program for Buckling and Postbuckling of Stiffened Laminated Curved Panels," *Computers and Structures*, Vol. 42, No. 1, 1992, pp. 87–95.

[3]Starnes, J. H., Jr., Knight, N. F., Jr., and Rouse, M.,"Postbuckling Behavior of Selected Flat Stiffened Graphite-Epoxy Panels Loaded in Compression," *AIAA Journal*, Vol. 23, No. 8, 1985, pp. 1236–1246.

[4]Lee, S., Elaldi, F., Villalobos, H., and Scott, R. F., "Experimental and Analytical Study of J-Stiffened Composite Panels Loaded in Axial Compression," *Proceedings of 9th International Conference on Composite Materials (ICCM-IX)* (Madrid, Spain), Woodhead Publishing, Cambridge, England, UK, 1993, pp. 519–526.

[5]Jun, S. M., and Hong, C. S., "Buckling Behavior of Laminated Composite Cylindrical Panel with Initial Imperfections," *Recent Developments in Buckling of Structures*, PVP-Vol. 183, AD-Vol. 18, American Society of Mechanical Engineers, New York, 1989, pp. 9–15.

[6]Kweon, J. H., and Hong, C. S., "An Improved Arc-Length Method for Postbuckling Analysis of Composite Cylindrical Panels," *Computers and Structures*, Vol. 53, No. 3, 1994, pp. 541–549.

[7]Kweon, J. H., Hong, C. S., and Lee, I. C., "Postbuckling Compressive Strength of Graphite/Epoxy Laminated Cylindrical Panels Loaded in Compression," *AIAA Journal*, Vol. 33, No. 2, 1995, pp. 217–222.